SLAC–PUB–12354
February 2007

A Theory for the RF Surface Field for Various Metals At the Destructive Breakdown Limit*

Perry B. Wilson
Stanford Linear Accelerator Center, Stanford University, Stanford, CA 94309

Author's Note

This is a slightly revised version of the paper that will be published in the AAC06 proceedings. A number of minor changes have been made in the interest of clarity. A significant revision, however, has been made in the treatment of backscattering of incident electrons from a metal surface. In the conference publication it was assumed that incident electrons were backscattered without energy loss. In this publication the energy spectrum of the backscattered electrons is taken into account. This revision does not significantly change the conclusions concerning the relative resistance of various metals to breakdown.

Invited tutorial presented at the 12th Advanced Accelerator Concepts Workshop (AAC06)
Lake Geneva, Wisconsin
July 10–15, 2006

---

*Work supported by US Department of Energy contract DE-AC02-76SF00515

A Theory for the RF Surface Field for Various Metals At the Destructive Breakdown Limit

Abstract. By destructive breakdown we mean a breakdown event that results in surface melting over a macroscopic area in a high E-field region of an accelerator structure. A plasma forms over the molten area, bombarding the surface with an intense ion current (~10^8 A/cm^2), equivalent to a pressure of about a thousand Atmospheres. This pressure in turn causes molten copper to migrate away from the iris tip, resulting in measurable changes in the iris shape. The breakdown process can be roughly divided into four stages: (1) the formation of "plasma spots" at field emission sites, each spot leaving a crater-like footprint; (2) crater clustering, and the formation of areas with hundreds of overlapping craters; (3) surface melting in the region of a crater cluster; (4) the process after surface melting that leads to destructive breakdown. The physics underlying each of these stages is developed, and a comparison is made between the theory and experimental evidence whenever possible. The key to preventing breakdown lies in stage (3). A single plasma spot emits a current of several amperes, a portion of which returns to impact the surrounding area with a power density on the order 10^7 Watt/cm^2. This power density is not quite adequate to melt the surrounding surface on a time scale short compared to the rf pulse length. In a crater field, however, the impact areas from multiple plasma spots overlap to provide sufficient power density for surface melting over an area on the order of 0.1 mm^2 or more. The key to preventing breakdown is to choose an iris tip material that requires the highest power density (proportional to the square of the rf surface field) for surface melting, taking into account the penetration depth of the impacting electrons. The rf surface field required for surface melting (relative to copper) has been calculated for a large number elementary metals, plus stainless-steel and carbon.

1. INTRODUCTION

By destructive breakdown we mean a breakdown event that results in surface melting over a macroscopic area in a high E-field region. A plasma forms over the molten area, bombarding the surface with an intense ion current (~ 10^8A/cm^2), which is equivalent to a pressure of about a thousand Atmospheres. This pressure causes molten copper to migrate away from the high-pressure region near the iris tip, resulting in changes in the iris shape that have a measurable effect on the rf properties of the structure.

The breakdown process occurs in four stages: (1) the formation of plasma spots and individual craters in high field regions on the metal surface; (2) setting up the condition for surface melting—crater clustering; (3) surface melting; (4) the process from surface melting to destructive breakdown.

2. THE FORMATION OF PLASMA SPOTS AND INDIVIDUAL CRATERS

1. Formation of Plasma Spots During Initial Processing

As the gradient in an accelerator structure is increased after the initial application of high power, sharp geometrical features in a high field region will begin to field-emit. At some field level, the tip of the projection will literally explode, injecting a jet or spray of liquid metal

droplets into the field above the projection. Field emission current quickly vaporizes and ionizes the droplets, leading to the formation of a plasma at the emitter site with a diameter on the order of a few microns. The plasma forms a Debye sheath at the point of contact with the metal. The sheath is a space charge limited Child's law diode, injecting electrons into the plasma and bombarding the surface below with an intense ion counter-current on the order of 10^8 A/cm^2, causing the metal below the spot to melt on a sub-nanosecond time scale. The molten area and associated plasma expand until the plasma quenches after some tens of nanoseconds. A small crater-like feature, with a diameter ~ 5–20 μm is left behind. Plasma spots form on metal surfaces in both rf and dc fields. The craters left behind are indistinguishable in the two cases.

The energy going into the formation of a crater is very small—only about 10^{-5} J. However, the electrons injected into the vacuum by a plasma spot (~ 10 A) pick up, on the average, perhaps one hundred keV of energy from the rf field. The energy extracted from the field in 30 ns is then on the order of 0.03 J. This is nearly sufficient to collapse the field in a cell of a typical standing-wave accelerator structure. However, in a traveling-wave structure energy flows into the cell at a higher rate and the rate of energy extraction by a single plasma spot is not sufficient to produce field collapse. Multiple closely spaced plasma spots can also form that extract more energy from the field. A substantial fraction of the electrons injected into the vacuum by a plasma spot return back to impact the surface near the spot (back-bombardment).

2. Some Possible Triggers for Plasma Spot Formation

Two models for plasma spot initiation have been investigated in some detail. In the mechanical breakup model proposed by Norem and his colleagues [1], the force due to the intense surface field at the tip of a projection exceeds the tensile strength of the metal, causing a fragment of the tip to break loose. Once this micro-particle has separated from the emitter tip, it is subjected to an intense electron bombardment by field emission electrons from the remaining tip. When the gap is comparable to the micro-particle diameter, the power per unit area (gap voltage times the field emission current per unit area) is sufficient to vaporize the micro-particle before it has had time to move away by its own diameter. The field emission electrons then ionize the metal vapor, leading to the formation of a plasma.

A variation in this scenario assumes that the tip of the emitter first begins to melt rather than break off. One might guess that I^2R heating could produce such melting. However, for an emitter tip with any reasonable geometry, diffusion carries away the heat almost as fast as it is produced. This is true even for a tip shaped like a cylinder with a ten-to-one height to diameter ratio, unless the cylinder has a sub-nanometer diameter. However, a tip-melting model that will work assumes a layer of adsorbed gas (O_2, CO, etc.) in the area surrounding the emitter or at a nearby grain boundary. Electron back-bombardment then produces electron-induced desorption of the gas. The gas moves away from the surface to the region of the tip, where field emission electrons ionize it. The ions then move back toward the tip, impacting the tip surface and heating it to the melting point.

The two models can be compared with experiment at several points. Experiments on field emitters in niobium superconducting cavities show that there is a fairly sharp upper limit of about 7 GV/m [2] that the surface field at the tip can reach before being destroyed by a breakdown event. At this field level the E^2 force pulling on the surface is roughly equal to the tensile strength of niobium, in agreement with the mechanical breakup model. Many emitters are observed to fail at considerably lower tip fields [2], but this could be due to the fact that the tip material is

mechanically weak because of fracturing, etc. In this model, the breakdown field is independent of tip area. The molten tip model the tip area is obtained by equating the outward E^2 force on a hemispherical segment capping a cone, with the restraining force around its perimeter due to surface tension. In a study of field emitters in superconducting cavities, Knobloch [3] has observed that starburst formation (indicating formation of a plasma) tends to occur at emitter areas between 10^{-15} and 10^{-16} m^2, corresponding to a tip radius of about 7 nm. At this critical radius the tip literally explodes, injecting metal vapor into the electron stream with subsequent ionization and plasma formation. The data is best explained by the assumption that the tip is in the liquid state. It is likely that both models apply to plasma spot formation on practical structure surfaces.

3. CRATER CLUSTERING—A PRECONDITION FOR SURFACE MELTING

1. Why Is Crater Clustering Necessary?

The area around a plasma spot subject to electron back-bombardment is on the order of 100 μm in diameter. The power per unit area produced by the impacting electrons is simply not enough to raise the surface temperature to the melting point on a 100 ns time scale. What is needed are a large number of closely spaced, active plasma spots within this same area. A crater field, consisting of hundreds of overlapping craters and dozens of plasma alive within the field, will provide sufficient power per unit area to melt the surface.

2. How Do Crater Clusters Form?

A crater left behind by the destruction of a field emitter looks somewhat like a volcano crater. Material that was thrown or pushed out from the central depression forms a jagged rim surrounding it. The sharply pointed features on the crater rim can themselves become field emitters. Also, there may be loosely attached debris in high field regions on the crater rim that can readily form plasmas spots following Norem's model. As the sharpest surface features are burned away during processing, it becomes more and more likely that new plasma spots will form on the rim of an existing crater, producing two overlapping craters. The total rim circumference of the two overlapping circular craters is larger (by a factor of 5*/3)* than the rim circumference of a single crater, making the probability still higher that a new plasma spot will form on the double crater. As more and more craters are added to the cluster, the probability of a hit continues to increase, although at a decreasing rate per additional crater. In this way clusters of hundreds of overlapping or closely spaced craters can form. Conditions are now ripe for dozens of plasma spots to be alive within the cluster during a time window of 30 ns or so. Electron back-bombardment from these closely spaced spots can now heat the entire cluster area and raise the temperature to the melting point in this time frame.

The images in Fig.1, showing the tip region of an iris in a TW accelerator structure, illustrate the process. Single isolated craters form in lower field regions away from the iris tip. Closer to the iris tip small crater clusters begin to form, and still closer larger clusters form. Finally, in the tip area itself smooth puddled regions, indicative of melting, are seen.

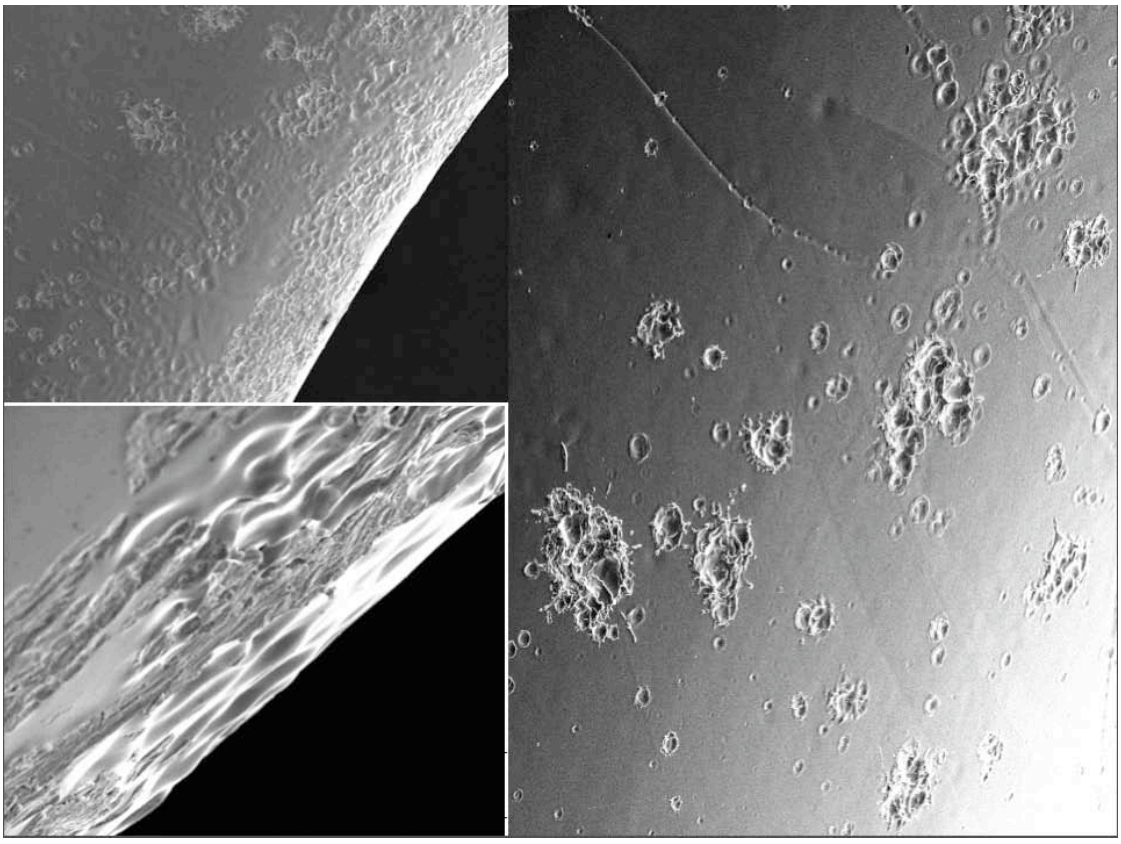

FIGURE 1. SEM images of the iris tip region of a traveling-wave structure after processing at the breakdown limit (courtesy of Chris Adolphsen, SLAC).

The process of crater clustering is illustrated even more clearly by the SEM image in Fig. 2. The image shows a surface that has been processed to about 400 MV/m at 150 ns in the Windowtron rf breakdown test apparatus at SLAC. For details see [4]. The high surface field is produced in a 1.4 mm gap between demountable re-entrant electrodes in an X-band klystron-like cavity. The field is nearly uniform over the test surface, in contrast to the large variation near an iris tip for the images in Fig.1. As seen in Fig. 2, there are numerous isolated single craters, several groups of two to a dozen craters, and about 15 clusters with more than a dozen craters. Clearly, most of the craters on the surface are members of a cluster. There is not enough electron bombardment power available in this particular cavity to melt the surface.

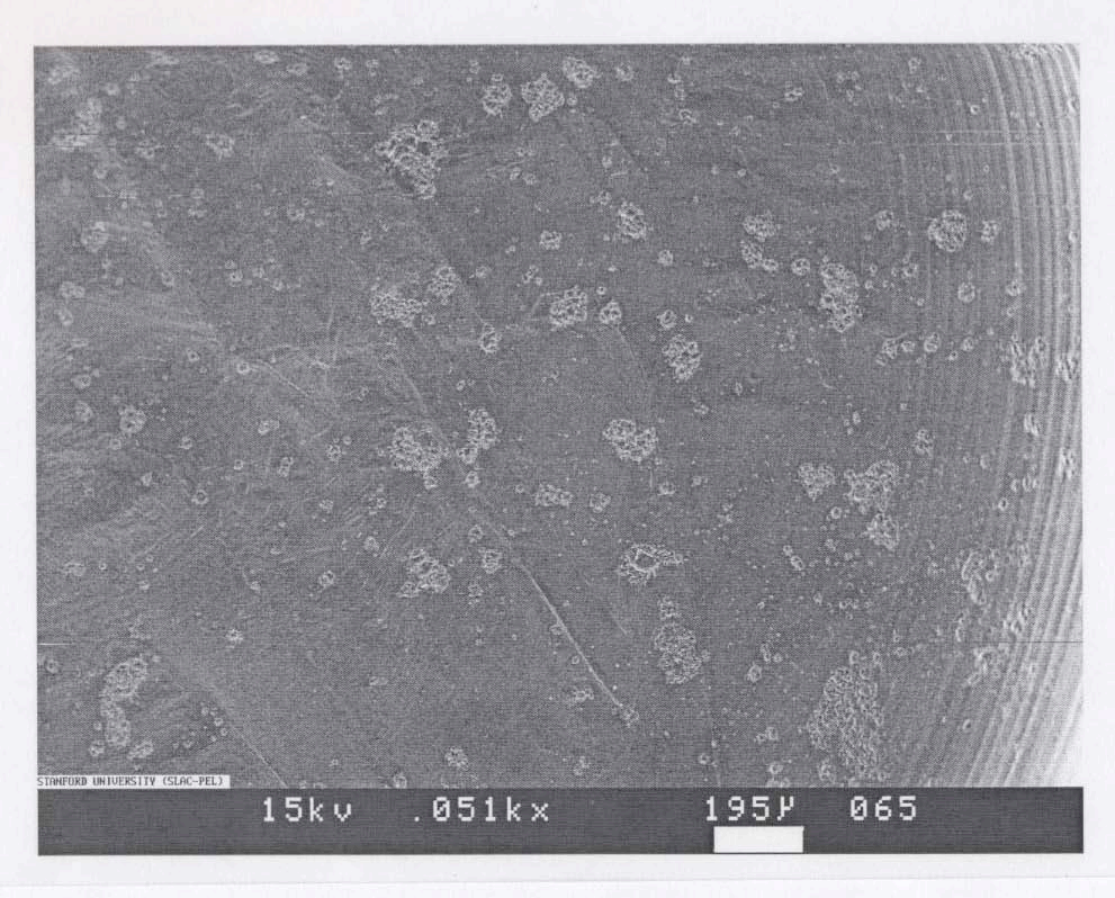

FIGURE 2. SEM image illustrating crater clustering (courtesy of Lisa Laurent, SLAC).

4. CALCULATION OF THE DESTRUCTIVE BREAKDOWN THRESHOLD

1. Penetration of Electrons into Metals

An electron with an energy in the keV range incident on a metal surface will produce a shower of scattered electrons that will penetrate a considerable distance into the metal. This distance depends on the energy of the incident electron and on the density of the metal. The images in Fig. 3 show Monte Carlo simulations for electron scattering and energy dissipation for a 25 keV electron incident on silicon, copper and gold targets [5]. Approximate penetration depths of the showers in microns are given in Table 1, along with the densities of these metals.

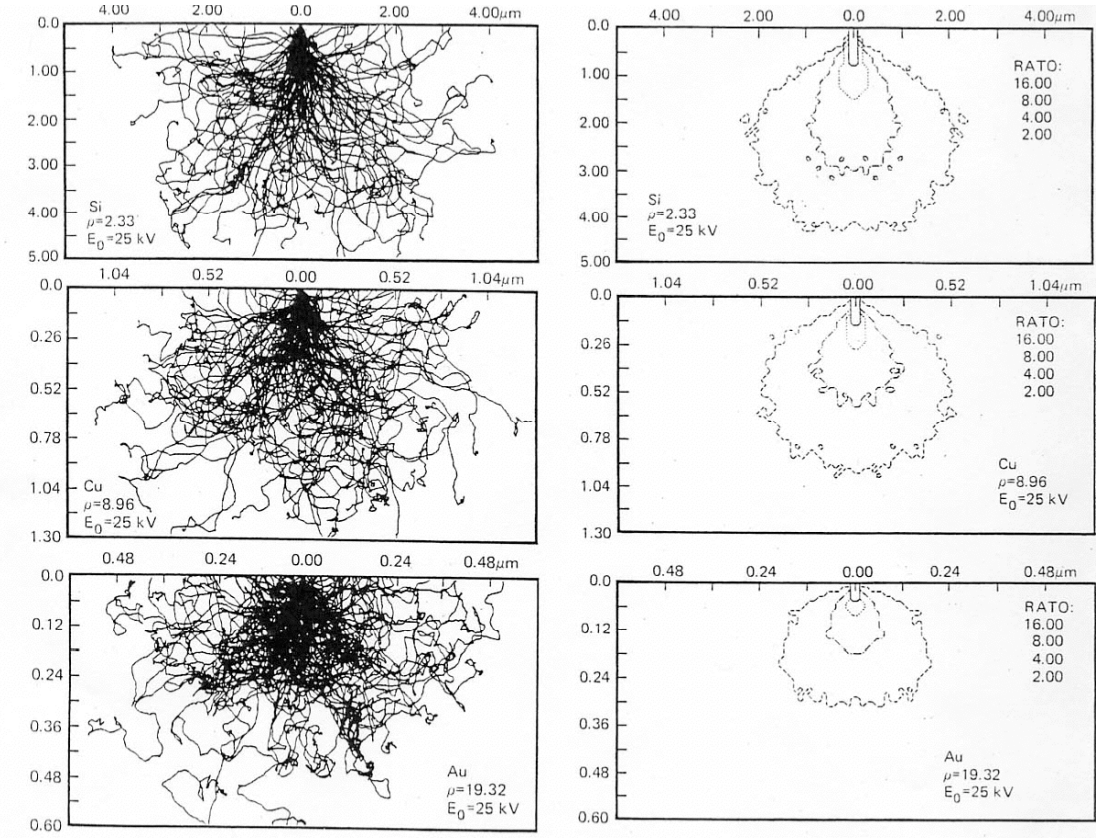

FIGURE 3. Monte Carlo simulations showing the shower produced by a 25 keV electron incident on silicon, copper and gold targets.

TABLE 1. Electron Penetration Depth for Silicon, Copper and Gold

Metal	Penetration Depth $X_0(\mu m)$	Density ρ (g/cm^3)	$X_0\rho$
Silicon	2.2	2.34	5.1
Copper	0.59	8.96	5.3
Gold	0.25	19.3	4.8

For a wide range of materials, the product of the penetration depth and the density is roughly constant. As a function of incident electron energy, the penetration depth varies approximately as $X_0 \sim V^{1.5}$ in the energy range of interest. Knowing the deposition of energy as function of depth and radial position from these Monte Carlo simulations, the surface temperature as a function of time can be computed from a solution of the 2D heat diffusion equation. However, an approximate solution can be obtained fairly easily from a 1D heat diffusion equation.

2. Calculation of the Temperature rise

Assumptions

1. The electron trajectories are normal to the surface and the reflection coefficient is independent of surface material.
2. The energy is deposited uniformly over the penetration depth.
3. All the incident electrons have the same energy.

Parameters and definitions

P_A (W/cm^2)—incident power/unit area. X_0 (cm)—penetration depth. C_s(J/g-°C)—specific heat. K(W/cm-°C)—thermal conductivity. D (cm^2/s) = $K/C_s\rho$—diffusivity. X_D (cm) = $(Dt)^{1/2}$—diffusion depth. T_m (°C)—melting point. T (°C)—surface temperature increase above 20°C. H (J/g)—heat of fusion.

Limits with simple solutions for the surface temperature rise

Penetration depth large compared to the diffusion depth:

$$T = P_A t/(X_0 \rho C_s) \sim P_A t/C_s \quad (X_0\rho \cong \text{constant}) \tag{1}$$

Penetration depth small compared to the diffusion depth:

$$T = P_A(2/\pi^{1/2})X_D/K \sim P_A t^{1/2}(D/K)^{1/2} \tag{2}$$

Solution for the general case at time t_0

$$T = \frac{P_A}{X_0 C_S \rho}\int_0^{t_0} erf\left\{\frac{X_0}{\left[4D(t_0 - t)\right]^{1/2}}\right\}dt \tag{3}$$

Recalling that $X_0\rho$ is approximately constant, the power per unit area at the melting point $T = T_M$ is proportional to

$$P_A \sim T_M C_S/I(t_0)$$

where $I(t_0)$ is the integral in Eq.(3).

We will want to melt the surface at the beginning of the rf pulse in a time which is a reasonably short fraction of the total pulse length. The main part of the pulse can then be spent in developing the geometric features discussed in Sec. 4. Assuming a total X-band pulse length in the range 100–400 ns, we'll somewhat arbitrarily pick t_0 = 30 ns. The breakdown field scales as $(P_A)^{1/2}$ giving

$$E_b \sim \left[\frac{T_M C_S}{I(30ns)}\right]^{1/2}$$

However, after the temperature is raised to the melting point, additional energy (the heat of fusion) must be applied to liquefy the metal. Consider the element of depth dx closest to the surface just as the surface reaches the melting point. As additional energy is supplied, the temperature of the metal in dx can no longer change, nor that of its neighboring element of material. Therefore, there is no temperature gradient close to the surface and the additional energy required to melt the material can be calculated without taking heat diffusion into account. Including the heat of fusion, the breakdown field scaling becomes

$$E_b \sim \left[\frac{T_m C_s}{(I/t_0)} + H \right]^{1/2} \qquad (4)$$

The dimensionless factor I/t_0 depends on the ratio of X_0/X_D. If this ratio is large, $I/t_0 \rightarrow 1$. If it is small, the first term in the brackets reduces to the correct value for diffusive heat flow.

One further simplification can be made. In standard texts on thermal physics [6] it is shown that the product of the specific heat and the atomic weight *A* of a metal is approximately constant. Except for a few metals with high Debye temperatures (e.g., beryllium), the constant is 24 J/g +/– 6%. In this approximation, $T_m C_s$ in the expression above can be replaced by $24\ T_m/A$.

3. Backscattering

A fraction of the electrons incident on the metal surface are backscattered. This fraction is the backscattering coefficient, given by [7]:

$$b = A + BZ + CZ^2 + DZ^3$$

where $A = -5.23791 \times 10^{-3}$; $B = 1.5048371 \times 10^{-2}$; $C = -1.67373 \times 10^{-4}$; and $D = 7.16 \times 10^{-7}$. The question arises as to whether some fraction of the backscattered electrons might return on the next rf cycle to contribute to surface heating. However, this is unlikely because almost all the backscattered electrons are ejected from the metal surface at angles greater than a few degrees. Because of their transverse velocity, these electrons will return displaced by an offset that is larger than the cluster diameter.

The backscattered electrons have energies ranging from the incident electron energy down to zero. A fraction of the backscattered electrons are reflected without energy loss by scattering from a single nucleus near the surface, while other electrons penetrate some distance into the material then back-diffuse to emerge again from the surface. A calculation of the energy spectrum of the backscattered electrons is given in [8]. The fraction of the incident electron energy carried away by backscattering is given by rb, where the factor r takes the energy spectrum into account (r = 1 if all the electrons have the incident energy). The power per unit area that is effective in producing heating is reduced by the factor (1 – rb). It follows that the expression for breakdown scaling given in Eq.(4) must modified by multiplying by $(1 - rb)^{-1/2}$.

The result of the calculation for most metals of interest is given in the Table 2. Beryllium, with an improvement factor over copper of 2.0, is clearly the all-star metal, although safety issues make it awkward to work with. Chromium, with an improvement ratio of 1.37, is easy to machine and can also be electroplated. Perhaps the most interesting material of all is carbon. There are at least two possible ways to obtain an iris tip with a carbon surface. First, an iris-tip ring can be machined from graphite. Because carbon is slightly conducting, the perimeter of the central hole in the ring can be electroplated with copper and this insert then brazed on the body of the iris. Second, a presentation at this workshop by Euclid Techlabs LLC shows that chemical vapor deposition of a diamond layer is also a possibility. The breakdown field groups in Table 2 are plotted on a periodic table of the elements in Fig. 4.

TABLE 2. Breakdown Fields Normalized to Copper for Various Metals

< 1.00	1.00 –1.09	1.10–1.19	1.20–1.29	1.30–1.39	> 1.4
Zn 0.64	Cu 1.00	Zr 1.10	SS 1.20	Re 1.30	Be 2.0
Au 0.80	Ca 1.03	Mn 1.11	Co 1.22	Sc 1.31	
Ag 0.83	Tc 1.07	Y 1.13	Os 1.26	Mo 1.34	*Non-metals*
Pt 0.89		Rh 1.13	Nb 1.27	Cr 1.36	Si 1.2
Hf 0.96		Ta 1.14	Ru 1.27	W 1.37	B 2.3
Pd 0.97		Al 1.14	Ti 1.29	V 1.39	C 3.7
		Mg 1.15			
		Ir 1.17			
		Fe 1.18			
		Ni 1.19			

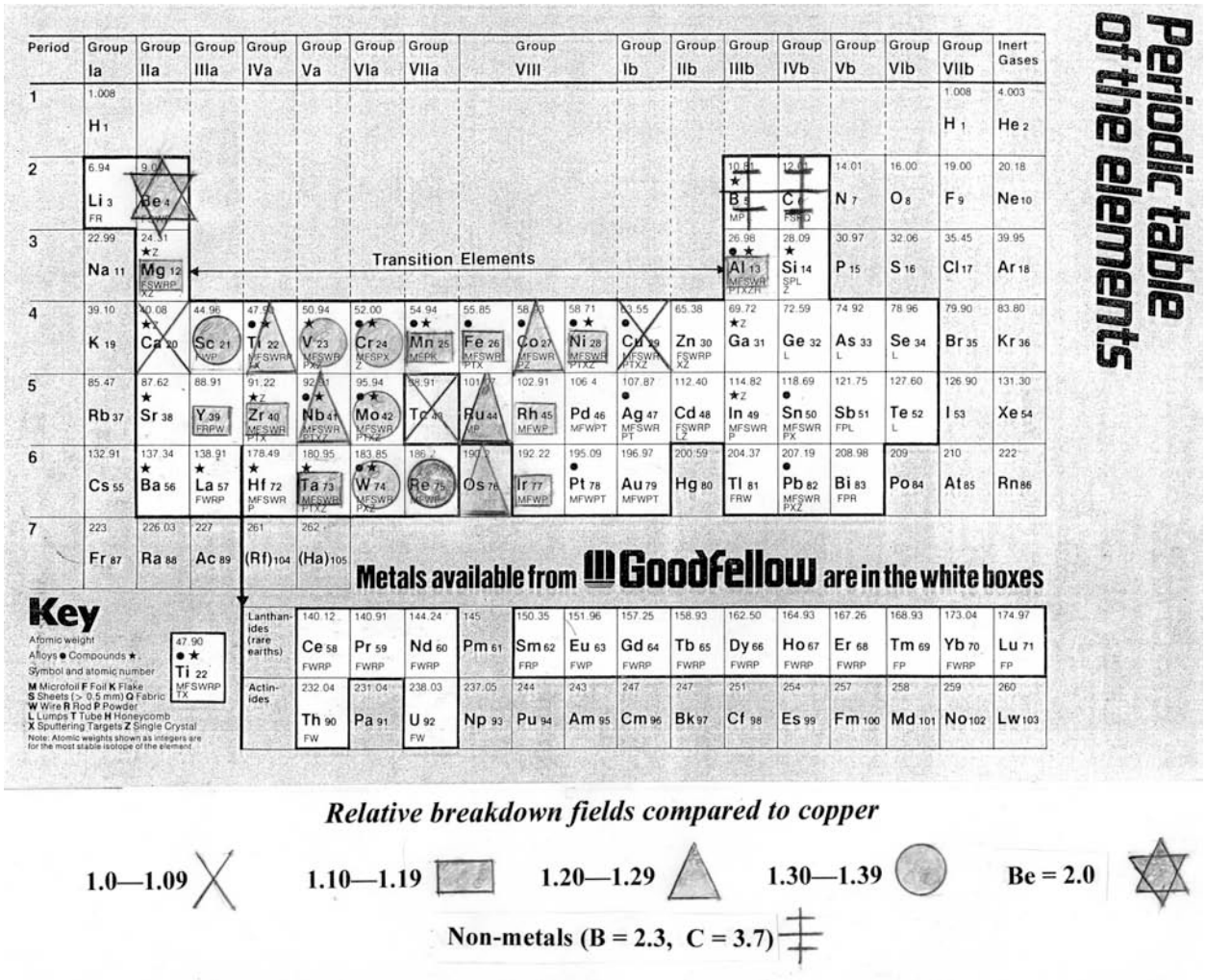

FIGURE 4. The breakdown field groups in Table 2 plotted on a periodic table of the elements [9].

5. FROM SURFACE MELTING TO DESTRUCTIVE BREAKDOWN

1. Some Comments on the Properties of Destructive Breakdown

Destructive breakdown forms an absolute limit on gradient. At this limit, macroscopic amounts of material are removed or displaced (the shape of an iris tip can be deformed without actual material removal). Measurements show that the threshold for catastrophic breakdown varies with pulse length as $1/(T_P)^{1/4}$ [10]. To first order, the threshold for destructive breakdown at the same pulse length for structures with the same geometry seems to be roughly independent of frequency for frequencies that are sufficiently high, although the experimental evidence for this is not yet conclusive. In this limit breakdown is a single surface phenomenon. The physics during the initial stage of destructive breakdown is independent of distant surfaces. The extent of the eventual damage does, of course, depend on macroscopic properties of the structure geometry, such as the energy available in a single structure cell.

2. Action of a DC Electric field on a Molten Metal Surface

The image in Fig. 5 shows the surface of a thin metal layer that has been melted and then cooled in an intense dc field.

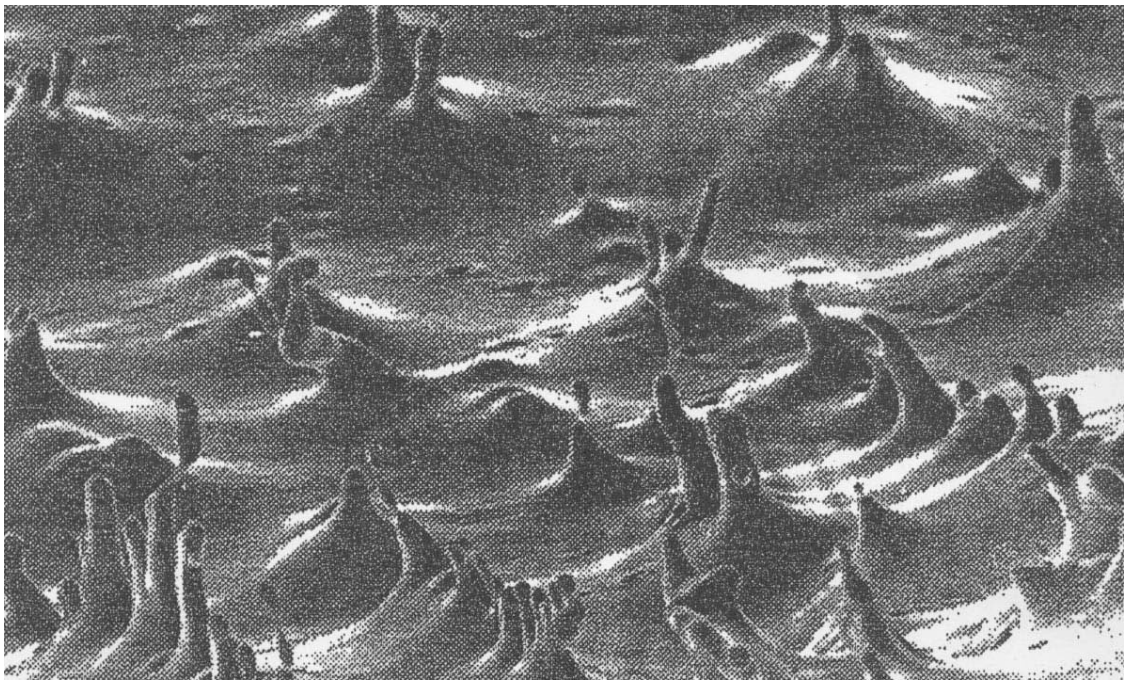

FIGURE 5. Image showing the growth of projections on a molten metal surface subjected to an intense dc electric field [11].

Note the cone-like features with a base angle of about 45°, with finger-like projections emerging from the apex of almost every cone. It is reasonable to assume that similar effects will take place for a molten surface in an rf field. To form these features starting with a relatively flat surface, material must be moved around mechanically—a slow process such that not much can happen during a sub-microsecond pulse. It will therefore take many such pulses to build up features like those shown above. As a first step, we'll build a theory for how these cones with projections jutting from their tops might form. We'll find that these features have a relationship to Kevlar bullet-proof vests, to some work in 1964 on the disintegration of water drops at the tip of a capillary in an electric field, and to liquid metal ion sources for ion beams.

3. Theory for the Growth of the Cones Shown in Fig. 5

We first model the growth of the cone before the projections emerge. We assume the apex of the cone is capped by a spherical segment of radius r. As the cones grow in height the radius becomes smaller until an instability threshold is reached, at which point the projections emerge. The nature of the instability will be discussed later.

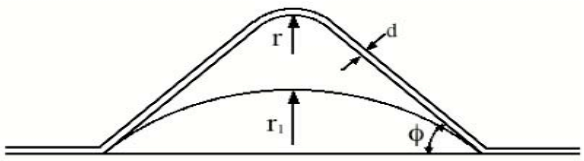

FIGURE 6. Model for the cones seen in Fig. 5.

Figure 6 is a model for the growth of a cone. We assume that growth starts from a shallow, rounded perturbation on the molten surface with radius r_1. The surface field E_s is enhanced at the apex of the perturbation, producing a pressure gradient between the apex and the base. This pressure gradient causes liquid metal to migrate toward the cone apex, causing the perturbation to grow. As the feature grows, the apex must maintain a roughly spherical shape. This is so because, since the surface is liquid, it must be in hydrostatic equilibrium. The external negative pressure (proportional to $r^2E_S^2$) on the surface must be balanced by the restraining force of surface tension pulling on the perimeter $2\pi r$. The resulting expression for the radius is

$$r = 8\alpha/\varepsilon_0 E_S^2,$$

where α is the surface tension (1.4 Nt/m for molten copper). As the height of the cone increases the radius of the cap decreases and the surface field and enhancement factor $\beta = E_S/E_0$ also increases. Simulations show that beta can be modeled as $\beta \sim r^{-n}$, where n is a function of the base angle ϕ. The radius of the molten cap varies as $r/r_1 = E_1^2/E_S^2$, giving $\beta = \beta_1 (r/r_1)^{-1/2}$, where β_1 is the value of beta at $r = r_1$. Simulations show that for n to be exactly ½, the base angle ϕ must be 41° with $\beta_1 \approx 1.9$. This is in agreement with some 1964 work by Taylor [12] on liquid droplets at the tip of a capillary exposed to an electric field. Some of Taylor's results are shown in Fig.7.

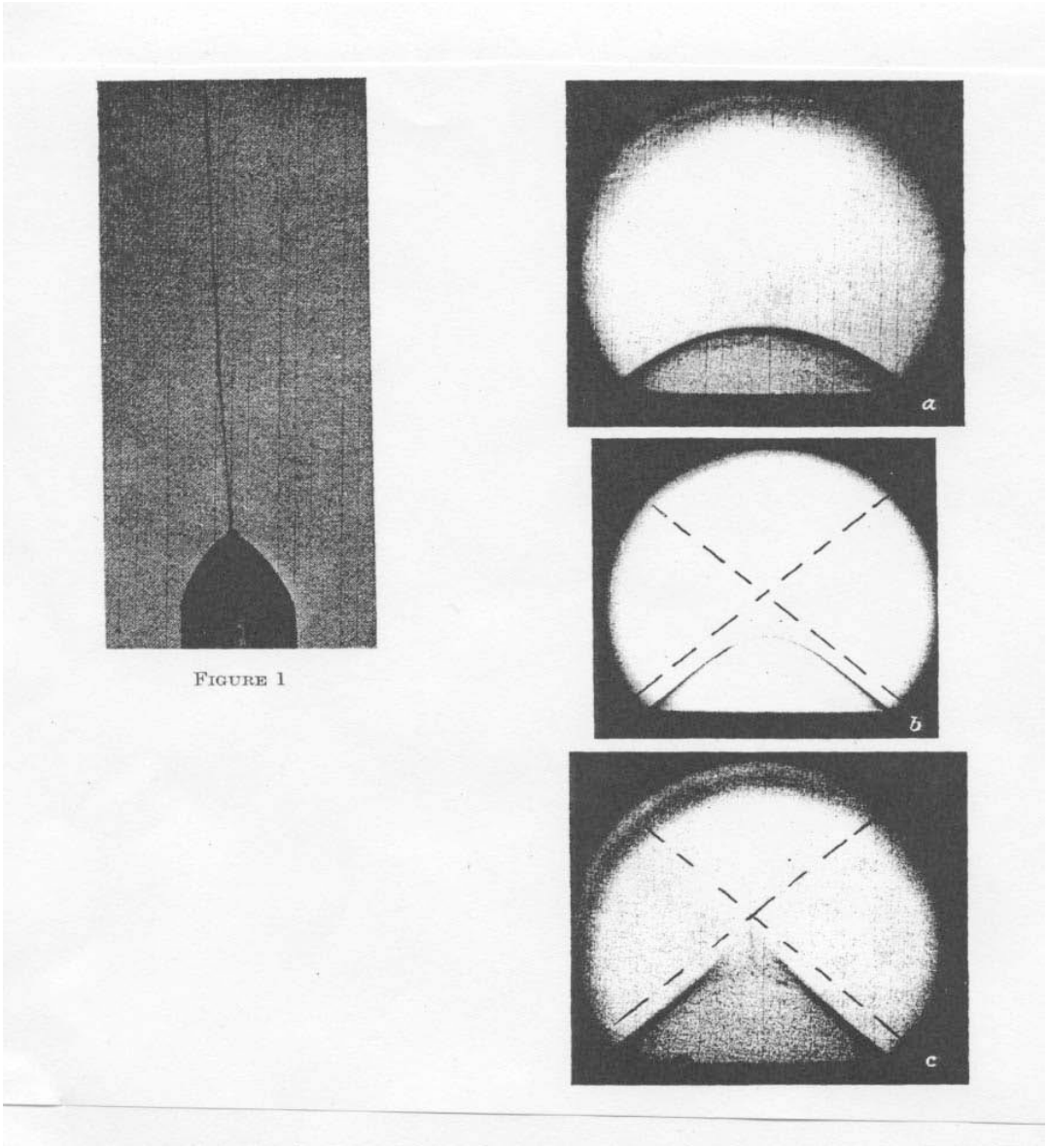

FIGURE 7. Insets *a* through *c* show the effect of an electric field of increasing strength on a water droplet at the tip of a glass capillary tube. In *c* the tip is in the process of disintegration. The inset at the left shows the emergence of a liquid jet from a glycerin droplet at the instability threshold [12].

As the electric field is increased (*a* through *c* above), the radius at the tip of the droplet decreases until an unstable point is reached. A jet of liquid is then seen shooting out from the tip in the case of glycerin (inset at the left) or a liquid spray for the case of water. At the point of the instability, the base angle of the cone in *c* is 40.7°. The cones produced by the action of a strong E-field on a liquid surface, including the surface of a molten metal, are called Taylor cones.

We next develop a model for the growth of the cone height with time. Assume a layer of molten metal of thickness d on the sides of the cone. The electric field pulling on the liquid surface increases from the bottom to the top of the cone—that is, there is an increasing negative pressure from bottom to top in the liquid layer. The liquid, flowing in the direction of lower internal pressure, then moves toward the top of the cone. A force of this type is often termed a ponderomotive force. The average flow velocity of the material in the liquid layer is calculated to

be $v = \varepsilon_0 E_S^2 d/8\eta$, where η is the viscosity. This can, in turn, be converted to a growth rate in cone height and hence in β. After a little algebra, we obtain

$$\beta = \frac{2}{\left[1 - BE_S^4 T\right]^{1/6}} \quad .$$

where $B \approx 6d^2\varepsilon_0^2/\alpha\eta r_1$ and T is the integrated time (repetition rate times the pulse length, with an initial melting time ~ 30 ns subtracted from the pulse length. Note that $E_0^4 T$ is a constant at the singularity, in agreement with experiment [10]. The details of the model could vary, but the scaling $E_S^4 T_{Pulse} = constant$ is robust.

Oh yes—bulletproof vests. Kevlar is made by exposing a molten layer of polymer on a metal plate to a strong electric field. As the field is increased, long strings of liquid with diameters ~10 nm suddenly emerge from the liquid surface (we'll postulate that the formation of these liquid strings follows the model illustrated by Fig. 5). The liquid strings cross the voltage gap and are laid down on a condensing plate in a random criss-cross pattern. Layers of these nanofibers form a cloth (Kevlar) with outstanding mechanical strength.

Taylor cones also form the basis for liquid-metal ion sources (LMIS) used in the production of high-resolution focused ion beams [13]. A LMIS consists of a liquid metal held in a suitable way to which a dc electric field is applied by a nearby positive "extraction" electrode. The field is strong enough so that the metal assumes a conical shape (Taylor cone). As the field is increased, the radius of the cone tip decreases and the surface field increases following the model above. At a sufficiently high surface field the cone tip begins to emit atoms by field evaporation. As explained in [13], field evaporation is a process in which an atom can evaporate from a surface on which the potential barrier against evaporation has been lowered by a strong field. The metal vapor can then be ionized by either field ionization [13], or alternatively by the flow of field emission electrons passing through it. The cone apex is believed to have a radius of only 5 nm.

6. A CONCLUDING COMMENT

The model presented here deals only with the ultimate surface field that can be reached on an iris tip without irreversible damage. The extent of the damage will depend on the rf energy available to feed the surface plasma covering the molten region, and this in turn depends on the global properties of the structure. In a real machine where a long structure life is required, one would want to allow an adequate overhead between the operating gradient and the ultimate gradient. Many breakdowns will of course occur while processing a structure up to the operating gradient. However, these breakdowns leave behind only single craters or clusters of craters that do not damage the surface in a way that changes the performance of the structure at the operating gradient. The present model has nothing to say about the probability for the occurrence of such breakdowns. My own guess is that field emitters on the surface are destroyed by melting due to ion bombardment beneath a plasma spot that forms over the emitter. In this case the temperature rise follows Eq.(2) on p.8. From this the amount of energy per pulse needed to destroy an emitter can be worked out. This energy per pulse should be related to the difficulty of processing a particular metal, and probably also to the breakdown rate as a function of pulse energy. Work on filling out the details for this model is in progress.

ACKNOWLEDGEMENTS

I would like to thank Gordon Bowden for getting this investigation of the physics of rf breakdown off on the right track by suggesting that I should begin by studying the extensive work already been done on dc breakdown (dc vacuum arcs). I would also like to thank Gordon for providing the solution to the heat equation given by Eq. (3), and Karl Bane for finding and evaluating an analytic solution to this equation. I have had many helpful discussions with Valery Dolgashev and Sami Tantawi on the physics underlying rf breakdown. Valery has also called several relevant references to my attention, in particular Ref. [7]. I would like especially to thank Valentin Ivanov for simulating the surface electric fields for the geometry of Fig. 6, and also for calling a key reference to my attention—Taylor's paper [12] on the disintegration of water droplets in an electric field. Finally, I'd like to thank Jim Norem for calling Ref. [13] to my attention.

REFERENCES

[1]. See for example A. Hassanein *et al.*, PRST-AB **9**, 062001 (2006).
[2]. H. Padamsee, J. Knobloch and T. Hays, *RF Superconductivity for Accelerators* (John Wiley & Sons, New York, 1998), Fig. 12.12.
[3]. Jens Knobloch, "Advanced Thermometry Studies of Superconducting Radio-Frequency Cavities" (Ph. D. Dissertation, Cornell University, 1997), Fig. 5.37.
[4]. Lisa Laurent, "High Gradient Breakdown Studies" (Ph. D Thesis, University of California, Davis, 2002).
[5]. David F. Kyser, "Monte Carlo Calculations for Electron Microscopy, Microanalysis and Microlithography" in D.F. Kyser, H. Niedrig, D.E. Newbury and R. Shimizu, eds., *Electron Beam Interactions with Solids* (SEM, Inc., AMF O'Hare, IL. 1982), p. 123.
[6]. See, for example F. Reif, *Fundamentals of Statistical and Thermal Physics*, McGraw-Hill, New York, 1965; Sec. 10.2.
[7]. G. Love and V. D. Scott, *J. Phys. D: Appl. Phys*. **11**, 1369 (1978).
[8]. Heinz Niedrig, "Analytic Models in Electron Backscattering" in D.F. Kyser, H. Niedrig, D.E. Newbury and R. Shimizu, eds., *Electron Beam Interactions with Solids* (SEM, Inc., AMF O'Hare, IL. 1982), p. 66.
[9]. Periodic table taken from Goodfellow US Catalog 7 (Goodfellow, Cambridge Science Park, Milton Road, Cambridge CB4 4DJ, England).
[10]. V. A. Dolgashev and S. G. Tantawi, "RF Breakdown in X-band Waveguides", EPAC 2002. Also SLAC-PUB-10355 (2002); Fig. 2.
[11]. G. A. Mesyats, *Explosive Electron Emission*, URO-Press, Ekaterinberg, 1998; p.29.
[12]. Geoffrey Taylor, *Proc. Roy. Soc. A*, **280**, 383 (1964).
[13]. Jon Orloff, High-resolution focused ion beams, Rev. Sci. Instrum. **64**, 1105 (1993).